

# Manipulation of molecular vibrations on condensing Er<sup>3+</sup> state-densities for 1.5 μm application

Huanqing Ye\*, Jelena Gorbaciova, Lyu Chen, Alex Walton, Khadisha Zahra, Richard J. Curry,  
Rex Bannerman, James Gates, Peter B. Wyatt, William P. Gillin\*

## Corresponding Author

**Huanqing Ye** - Chromosol Ltd, The Walbrook Building, 25 Walbrook, London, EC4N 8A, U.K.; Email: [huanqing.ye@chromosol.com](mailto:huanqing.ye@chromosol.com)

**William P. Gillin** - Materials Research Institute and Department of Physics and Astronomy, Queen Mary University of London, Mile End Road, London, E1 4NS, U.K.; Chromosol Ltd, The Walbrook Building, 25 Walbrook, London, EC4N 8A, U.K.; Email: [w.gillin@qmul.ac.uk](mailto:w.gillin@qmul.ac.uk)

## Authors

**Jelena Gorbaciova** - Chromosol Ltd, The Walbrook Building, 25 Walbrook, London, EC4N 8A, U.K.

**Jelena Gorbaciova, Lyu Chen** - Materials Research Institute and Department of Physics and Astronomy, Queen Mary University of London, Mile End Road, London, E1 4NS, U.K.

**Alex S. Walton, Khadisha M. Zahra** - Photon Science Institute and Department of Chemistry, FSE Research Institutes, The University of Manchester, Manchester, M13 9PL, U.K.

**Richard J. Curry** -, Department of Electrical and Electronic Engineering, University of Manchester, Manchester M13 9PL, UK

**Peter B. Wyatt** - Materials Research Institute and Department of Chemistry, Queen Mary University of London, Mile End Road, London E1 4NS, U.K.

**Rex Bannerman, James Gates** - Zepler Institute, Faculty of Engineering and Physical Sciences, University of Southampton, Southampton, SO17 1BJ, U.K.

**ABSTRACT.** The vibrational modes of chemical bonds in organic erbium ( $\text{Er}^{3+}$ ) materials play an important role in determining the efficiency of the  $1.5 \mu\text{m}$   $\text{Er}^{3+}$  emission. This work studies the energy coupling of the  $\text{Er}^{3+}$  intra-4f transitions and vibrational modes. The results demonstrate that the coupling introduces enormous nonradiative internal relaxation which condenses the excited erbium population on to the  ${}^4\text{I}_{13/2}$  state. This suggests that vibrational modes can be advantageous for optimizing the branching ratio for the  $1.5 \mu\text{m}$  transition in organic erbium materials. Through control of the quenching effect on to the  ${}^4\text{I}_{13/2}$  state and a reliable determination of intrinsic radiative rates, it is found that the pump power for population inversion can be reduced by an order of magnitude at high erbium concentrations compared to conventional inorganic erbium materials.

## **TOC GRAPHICS**

## **KEYWORDS**

Organic Photonics; Vibrational Relaxations; Dynamic Equivalent; Population Inversion.

Silicon photonic integrated circuits (PICs) are set to pave the way for ultra-high-speed optic communications, and integrated light sources will play vital roles in producing gain regions on these PICs.<sup>1-4</sup> Hybrid III-V silicon integration is the current preferred approach, however there are still issues regarding their large-scale application in PICs. This inability to integrate optical gain effectively limits the complexity of PIC architectures that can be achieved. Rare-earth ion containing materials, particularly erbium ( $\text{Er}^{3+}$ ), are obvious candidates as the 1.5  $\mu\text{m}$  emission of  $\text{Er}^{3+}$  ions matches the low-loss telecommunication window (C-band).<sup>5-8</sup> Inorganic erbium doped materials have been widely suggested but  $\text{Er}^{3+}$  solubility is commonly low and there is usually quenching at even modest ion concentrations due to energy transfer up-conversion (ETU) between clusters of ions.<sup>9-12</sup> Although efforts have been made to increase the solubility, to increase gain capacity in a short length,<sup>13-16</sup> the weak absorption cross-section ( $10^{-21}$  to  $10^{-20}$   $\text{cm}^2$ ) of  $\text{Er}^{3+}$  ions remains a drawback as high excitation powers are required to reach population inversion resulting in high pump power densities on the end facet.<sup>12,17-19</sup>

Organic erbium materials contain organic chromophores that strongly absorb visible light to sensitize  $\text{Er}^{3+}$  excitations so as to reduce excitation power by orders of magnitude,<sup>20-22</sup> and approaches include polymers<sup>23,24</sup>, single molecules<sup>25-27</sup> and molecular composites/hybrids.<sup>28-</sup>

<sup>31</sup> This sensitisation means that ideally a cheap and incoherent light source (LED or integrated OLED) illuminating from the top can be used to pump organic erbium waveguides on a compact scale. In contrast to inorganic erbium materials, where the photoexcitation is into the  $^4\text{I}_{13/2}$  or  $^4\text{I}_{11/2}$  states, organic sensitizers usually have exciton energies  $> \sim 2$  eV which will sensitize to energy states of  $\text{Er}^{3+}$  ions above the  $^4\text{I}_{11/2}$  level. As some of these higher energy states are efficient visible emitters themselves, it is unknown what impact this will have on the  $^4\text{I}_{13/2}$  level that is crucial for 1.5  $\mu\text{m}$  emission. We study the dynamic equilibrium of excited  $\text{Er}^{3+}$  states in an organic erbium molecule by investigating the coupling of vibrational modes of chemical bonds and the  $\text{Er}^{3+}$  intra-4f transitions. The results demonstrate that molecular

vibrations efficiently condense the excited states down to the  ${}^4I_{13/2}$  state with virtually no emission in the visible, with consequent advantages for 1.5  $\mu\text{m}$  applications.

Organic hosts usually have challenges in producing optical gain because the high vibrational energy of hydrogenated bonds (C-H, OH, or N-H) cause serious nonradiative quenching of the  $\text{Er}^{3+} {}^4I_{13/2}$  state that limits the internal quantum efficiency (IQE) to below 0.1%.<sup>32,33</sup> Fully-fluorinating organic bonds are a solution to effectively lower the vibrational energy to reduce quenching of the first excited state. Erbium (III) tetrakis(pentafluorophenyl)-imidodiphosphate,  $\text{Er}(\text{F-TPIP})_3$ <sup>28,34</sup> is used because the rare-earth complexes of this ligand show high thermal stability, to allow for thermal deposition of thin films, which are vital for the coverage of PIC structures. The molecular structure shows a ligand cage keeping the central  $\text{Er}^{3+}$  ion at least 1.4 nm from any other  $\text{Er}^{3+}$  ion and hence reducing ion-ion interactions and the consequent ETU. This is despite the fact that  $\text{Er}(\text{F-TPIP})_3$  has an  $\text{Er}^{3+}$  ion concentration of  $\sim 5 \times 10^{20} \text{ cm}^{-3}$ . However, its molecular nature makes it a challenge to accurately quantify the optical properties, such as the absorption cross-section for the  $\text{Er}^{3+} {}^4I_{13/2}$  state, as large area bulk crystals are difficult to fabricate. The determination of this parameter needs the determination of the absorption coefficient with an accurate optical path length, integration of the spectra with minimal interference from the background, refractive indices at the C-band, molecular concentrations, etc. Furthermore, hydrogenated impurities would introduce wavelength-dependent backgrounds which overlap the  $\text{Er}^{3+}$  spectral features and even distort the local ligand environment to affect the oscillator strength. Hence, measurements on solutions are not reliable, and measurements on thin films are also inaccurate as, not only is the absorption coefficient of  $\text{Er}^{3+} {}^4I_{15/2} \rightarrow {}^4I_{13/2}$  transition is too small, but also because there will be strong thin-film optical interference. Utilizing integrated spheres based on a fluorescence reference is suggested<sup>35</sup>, however the detection of weak  $\text{Er}^{3+}$  1.5  $\mu\text{m}$  spontaneous emission are likely to have larger uncertainties than for materials that emit in the visible with larger cross-sections.

We undertake direct measurements of the  $\text{Er}^{3+} \ ^4\text{I}_{15/2} \rightarrow \ ^4\text{I}_{13/2}$  absorption on a series of  $\text{Er}(\text{F-TPIP})_3\text{:KBr}$  pellets varying the weight concentrations of  $\text{Er}(\text{F-TPIP})_3$ . In order to subtract the background derived from the  $(\text{F-TPIP})_3$  ligand environment, we use a series of  $\text{Y}(\text{F-TPIP})_3\text{:KBr}$  pellets as reference backgrounds that contain similar weight concentrations of  $\text{Er}(\text{F-TPIP})_3$ , where  $\text{Y}^{3+}$  refers to optically inert yttrium (III) ions. To minimise the effect of KBr powder on the  $\text{Er}^{3+}$  spectral feature,  $\text{Er}(\text{F-TPIP})_3$  weight concentrations are employed with 75wt%, 94wt% and 100wt% to have the  $\text{Er}^{3+}$  signals clearly stronger than scattered backgrounds. An average absorption cross-section spectrum is shown in **Figure 1a**. The integral of the absorption cross-section spectrum ( $\sigma[\ ^4\text{I}_{15/2} \rightarrow \ ^4\text{I}_{13/2}]$ ) shows a linear response to the  $\text{Er}(\text{F-TPIP})_3$  concentrations. The refractive index at 1.55  $\mu\text{m}$  of  $\text{Er}(\text{F-TPIP})_3$  was measured using a Prism coupler on 3  $\mu\text{m}$  thin-films thermally evaporated on to a silicon wafer. Fitting the data [See Supplementary information (SI)] gives a radiative rate ( $k_{\text{rad}}[\ ^4\text{I}_{13/2} \rightarrow \ ^4\text{I}_{15/2}]$ ) of  $354 \pm 12 \text{ s}^{-1}$  for the  $\text{Er}^{3+} \ ^4\text{I}_{13/2} \rightarrow \ ^4\text{I}_{15/2}$  transition. This number is larger than that reported on a micro-size crystal of  $\text{Er}(\text{F-TPIP})_3$  precipitated from a DMSO solution.<sup>36</sup> The inaccuracy for crystal samples can be attributed to uncertainties in determining the refractive indices, the measured thickness, the full spectral width and the effect on the spectral background due to hydrogenated impurities.

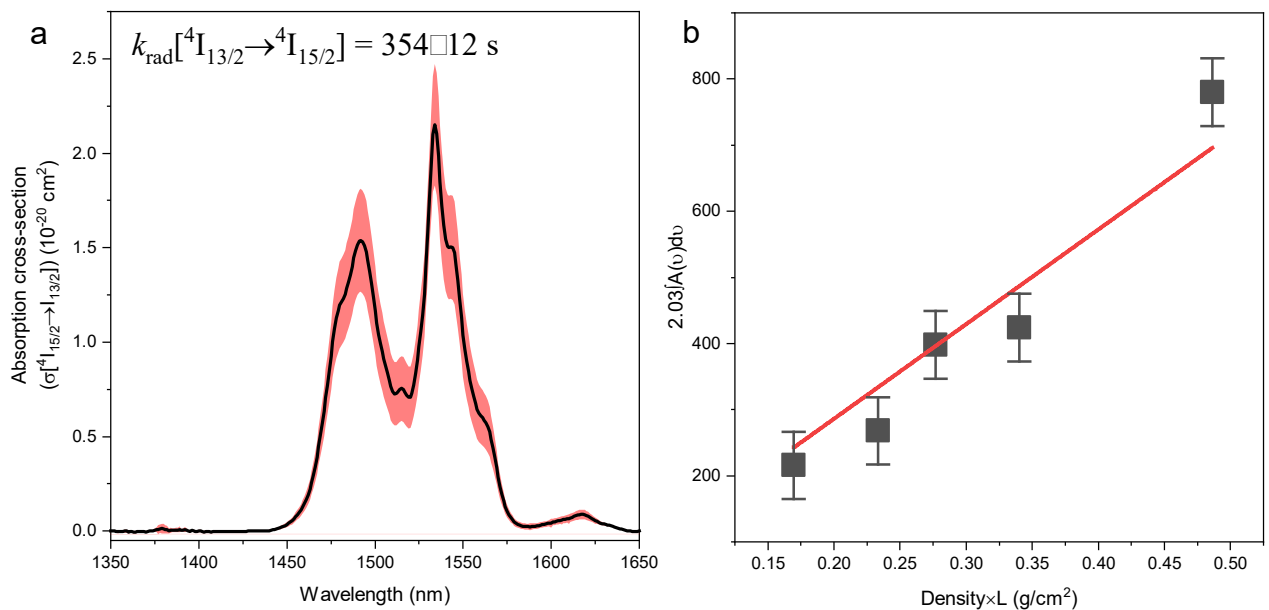


**Figure 1.** (a) The spectrum of the average absorption cross-section of  $\text{Er}(\text{F-TPIP})_3$  in KBr pellets. Error bars on the Y-axis are colour filled. (b) Fitting the integral of the absorbance spectra against various  $\text{Er}(\text{F-TPIP})_3$  densities multiplied by the optical path.

Once the intrinsic radiative rate is known one only has to measure the 1.5  $\mu\text{m}$  emission lifetime to determine the IQE of the  $^4\text{I}_{15/2} \rightarrow ^4\text{I}_{13/2}$  transition. As was reported for  $\text{Yb}(\text{F-TPIP})_3$ ,<sup>37</sup> it is vital to keep water vapour in the air from diffusing into the material in order to obtain the natural radiative lifetime. Hence, we fabricate thin films in a thermal evaporation system pumped by a cryopump to a ultra-high-vacuum (UHV) condition. Under such conditions, we minimise the chance of water molecules being trapped in the films during growth. The thin films are deposited on to polished silica substrates and a 500 nm thick aluminium layer is deposited after as an encapsulation. The encapsulated film sample gives a 1.5  $\mu\text{m}$  PL lifetime of  $0.97 \pm 0.1$  ms using direct excitation into the  $\text{Er}^{3+} \ ^2\text{H}_{11/2}$  level. Diluting  $\text{Er}(\text{F-TPIP})_3$  to 20% in a  $\text{Er}_{0.2}\text{Y}_{0.8}(\text{F-TPIP})_3$  composite film (with encapsulation) gives a PL lifetime of  $1.04 \pm 0.10$  ms (**Figure 2a**). This demonstrates that there is negligible quenching due to either energy migration or ion-ion interactions in the neat  $\text{Er}(\text{F-TPIP})_3$ . Therefore, the shell of the  $(\text{F-TPIP})_3$  ligands, keeping any two  $\text{Er}^{3+}$  ions separated by at least 1.4 nm, prevents the  $\text{Er}^{3+}$ - $\text{Er}^{3+}$  ion pairs that limit the performance of erbium containing glasses at high Er concentrations. These result shows that we could optimize the IQE for 1.5  $\mu\text{m}$  PL to be  $\sim 35\%$  with good control of fabrication conditions. Without encapsulation the PL lifetime is dramatically quenched and has two components with lifetimes of  $0.31 \pm 0.07$  ms (75% component) and  $0.65 \pm 0.02$  ms (25% component). Long term exposure of an unencapsulated film to air results in the lifetime becoming single exponential with a lifetime of  $\sim 200$   $\mu\text{s}$ . As this lifetime can be increased if the sample is measured in vacuum, and return to this value when exposed to air, we believe that the indiffusion of water molecules into the film is the most likely cause. Assuming Förster energy transfer between the excited  $^4\text{I}_{13/2}$  level and a random distribution of water molecules in

the film we were able to estimate a water concentration in the film of  $\sim 8 \times 10^{20} \text{ cm}^{-3}$  (see the SI for details) and a Förster radius of  $\sim 0.97 \text{ nm}$ . These values have a very large uncertainty (and are almost certainly an overestimate) due to the approximations used but with a Förster radius larger than the radius of an  $\text{Er}(\text{F-TPIP})_3$  molecule ( $\sim 0.7 \text{ nm}$ ) and implies that there is less than, but of the order of, one water molecule present in the film for every  $\text{Er}(\text{F-TPIP})_3$  molecule. We have used x-ray photoelectron spectroscopy (XPS) to look at the O 1s peak in similar films of  $\text{Er}(\text{F-TPIP})_3$ . These results show that there are two environments for the oxygen. The major peak corresponds to the P=O bonds in the  $\text{Er}(\text{F-TPIP})_3$  molecule, whilst a high energy shoulder is consistent with the binding energy for water. Taking the ratio of these two peaks we can obtain a water concentration that is about 25% of the Er concentration. Given that we have seen that water appears to diffuse from the films on exposure to vacuum these results are comparable to the Förster calculations and imply that without encapsulation a significant amount of water is present in the films and is responsible for quenching.

Organic luminescent chromophores are widely used as sensitizers, and these will populate the higher excited  $\text{Er}^{3+}$  ( $^2\text{H}_{11/2}$ ,  $^4\text{S}_{3/2}$  and  $^4\text{F}_{9/2}$ ) states. To investigate the internal relaxations within these states we use a 377 nm laser to directly excite the  $^2\text{G}_{9/2}$  state and the  $\text{Er}^{3+}$  PL spectrum is shown in **Figure 2b**. The calculated branching ratios for relaxations from the  $^4\text{G}_{11/2}$  to the lower states were calculated from a Judd-Ofelt (JO) analysis and are listed in **Table S2**.<sup>36,38–40</sup> **Figure 2b** also shows the calculated theoretical emission intensities of the  $^2\text{H}_{11/2}$ ,  $^4\text{F}_{9/2}$ ,  $^4\text{I}_{9/2}$  and  $^4\text{I}_{11/2}$  states, from the JO analysis and are the emissions expected with no internal quenching, normalized to the  $^4\text{I}_{13/2}$  emission intensity. It can be seen that the emission from the  $^2\text{H}_{11/2}$ ,  $^4\text{F}_{9/2}$ ,  $^4\text{I}_{9/2}$  have all disappeared (even when the scale is multiplied by a factor of 100), whilst the

emission from the  $^4I_{11/2}$  level is  $<0.5\%$  of that expected when compared to the intensity of the  $^4I_{13/2}$  emission.

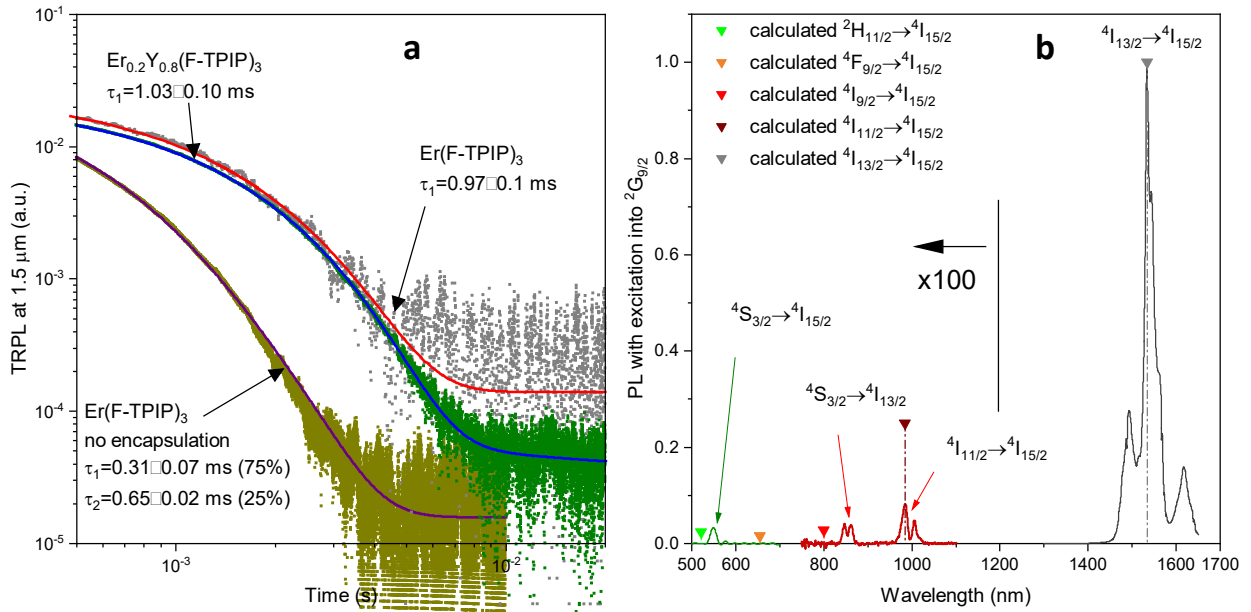


**Figure 2.** (a) Comparisons of TRPL spectra of Er(F-TPIP)<sub>3</sub> thin films with dilution, encapsulations, and no encapsulations. (b) The experimental Er(F-TPIP)<sub>3</sub> PL spectrum with excitation into <sup>2</sup>G<sub>9/2</sub>. The PL spectra below 1200 nm is magnified by 100 times. The theoretical normalised intensities of the transitions are indicated as coloured triangles with drop lines. Note that these are on the original scale and hence the PL is  $>100$  times weaker than expected.

We attribute this difference in the emission intensities to strong coupling with vibrations of the chemical bonds in the molecule. The FTIR spectrum of Er(F-TPIP)<sub>3</sub> powder shows vibrational features at wavenumbers below 1000 cm<sup>-1</sup> and **Figure 3** shows that the fundamental, 1<sup>st</sup> and 2<sup>nd</sup> overtones of the vibrational spectra overlap the energy gap of several of the internal transitions such as  $^2H_{11/2} \rightarrow ^4S_{3/2}$ ,  $^2H_{11/2} \rightarrow ^4F_{9/2}$ ,  $^4F_{9/2} \rightarrow ^4I_{9/2}$ ,  $^2I_{9/2} \rightarrow ^4I_{11/2}$  and  $^2I_{11/2} \rightarrow ^4I_{13/2}$ . This overlap suggests that nonradiative or thermal relaxations should be inevitable and hence we have used a Förster analysis to quantify them. **Figure 3a** shows the simulated molar absorption coefficients of the overtone vibrations. The peak absorption cross-section of the C=C stretch is between  $\sim 5 \times 10^{-20}$  to  $\sim 1 \times 10^{-19}$  cm<sup>2</sup>.<sup>41-43</sup> Hence, we can evaluate the peak absorption cross-section of C=C stretch at 1476 cm<sup>-1</sup> as within the range,<sup>41,44</sup> and convert the number to the



molar absorption coefficient on the FTIR spectrum of the fundamental overtone. Furthermore, we simulate the molar absorption coefficients of the 1<sup>st</sup> to 2<sup>nd</sup> overtone spectra, using reported empirical results that suggest that the amplitude of overtone vibrations will decrease by an order of the magnitude.<sup>44</sup>

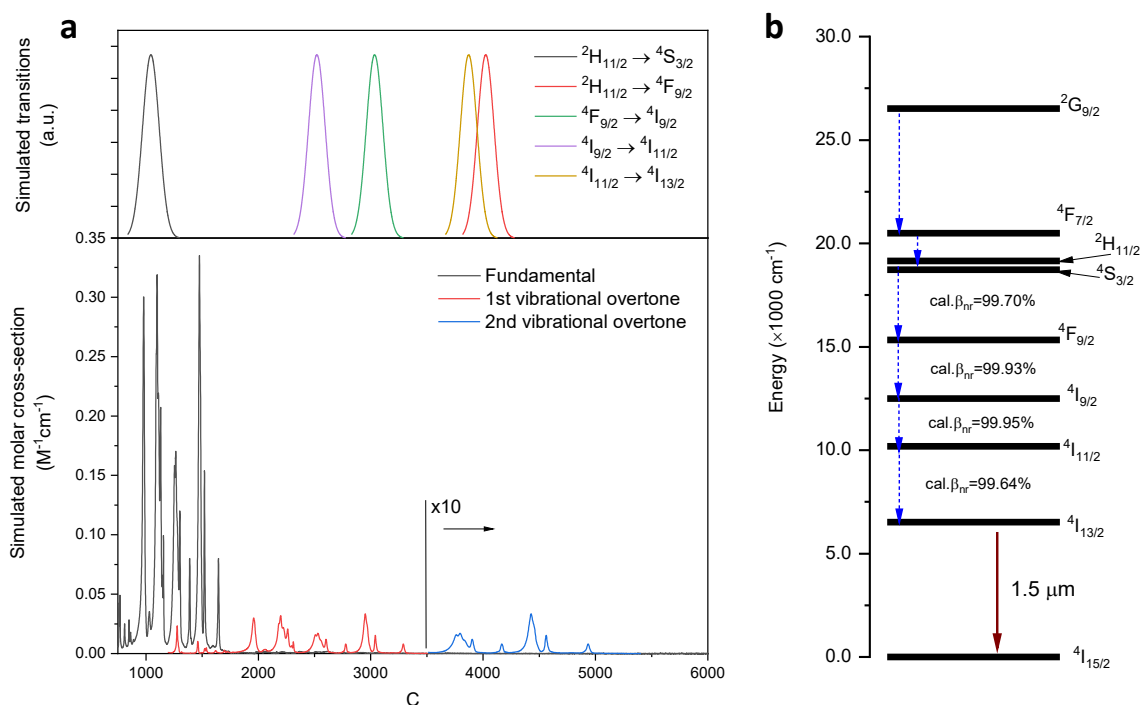


**Figure 3.** (a) The overlap of the vibrational and overtone (1<sup>st</sup>, 2<sup>nd</sup>) spectra and the simulated normalized spectra of the  ${}^4I_{11/2} \leftrightarrow {}^4I_{13/2}$ ,  ${}^4I_{9/2} \leftrightarrow {}^4I_{11/2}$ ,  ${}^4F_{9/2} \leftrightarrow {}^4I_{9/2}$  and  ${}^2H_{11/2} \leftrightarrow {}^4F_{9/2}$  transitions. (b) Calculated branching ratios for nonradiative transitions. The dashed arrows indicate the nonradiative relaxation.

According to the reported crystallographic data of  $\text{Er}(\text{F-TPIP})_3$ <sup>[34]</sup>, the molecular radius is ~ 0.7 nm and it suggests an effective Förster radius between vibrational bonds on the ligand and the  $\text{Er}^{3+}$  ions would be at most this radius. Therefore, using 0.7 nm as a Förster radius we can calculate the nonradiative rates for the  ${}^2H_{11/2} \rightarrow {}^4S_{3/2}$ ,  ${}^2H_{11/2} \rightarrow {}^4F_{9/2}$ ,  ${}^4F_{9/2} \rightarrow {}^4I_{9/2}$ ,  ${}^4I_{9/2} \rightarrow {}^4I_{11/2}$  and  ${}^2I_{11/2} \rightarrow {}^4I_{13/2}$  transitions. The results, when compared to the corresponding radiative transition rates, show that the non-radiative rates are orders of magnitude larger, as listed in **Table S2**. It

needs to be noted that the actual Förster radius might be significantly smaller than the molecular radius so that those nonradiative transition rates could be even higher than the simulated results. Nevertheless, these simulated values mean the population at these excited states will rapidly undergo nonradiative transitions to the  $^4I_{13/2}$  state with the branching ratios ( $\beta_{nr}$ ) for these non-radiative relaxations of  $> 99\%$ . This performance shows a clear difference compared to inorganic erbium materials such as  $Er^{3+}$ -doped nanoparticles, where green  $\sim 522$  nm ( $^2H_{11/2} \rightarrow ^4F_{9/2}$ ), red  $\sim 655$  nm ( $^4F_{9/2} \rightarrow ^4I_{9/2}$ ) and NIR  $\sim 980$  nm ( $^2I_{9/2} \rightarrow ^4I_{11/2}$ ) emission are particularly bright. In particular for the hypersensitive  $^2H_{11/2}$ , its intrinsic high branching ratio for  $^2H_{11/2} \rightarrow ^4I_{15/2}$  is replaced by a rapid relaxation to  $^4S_{3/2}$  followed by a 99.7% non-radiative relaxation towards  $^4F_{9/2}$ . It is interesting that we can still observe weak PL at  $\sim 534$  nm and  $\sim 850$  nm and their energies match the  $^4S_{3/2} \rightarrow ^4I_{15/2}$  and  $^4S_{3/2} \rightarrow ^4I_{13/2}$  transitions, respectively. Due to the strong interaction between the  $^2H_{11/2} \rightarrow ^4S_{3/2}$  transition and the molecular absorption there is complete relaxation to the  $^4S_{3/2}$  level. The  $^4S_{3/2} \rightarrow ^4F_{9/2}$  transition is “only” 99.7% quenched and hence there is some population on the  $^4S_{3/2}$  which allows the  $^4S_{3/2} \rightarrow ^4I_{15/2}$  and  $^4S_{3/2} \rightarrow ^4I_{13/2}$  transitions to be experimentally observed with low intensity.

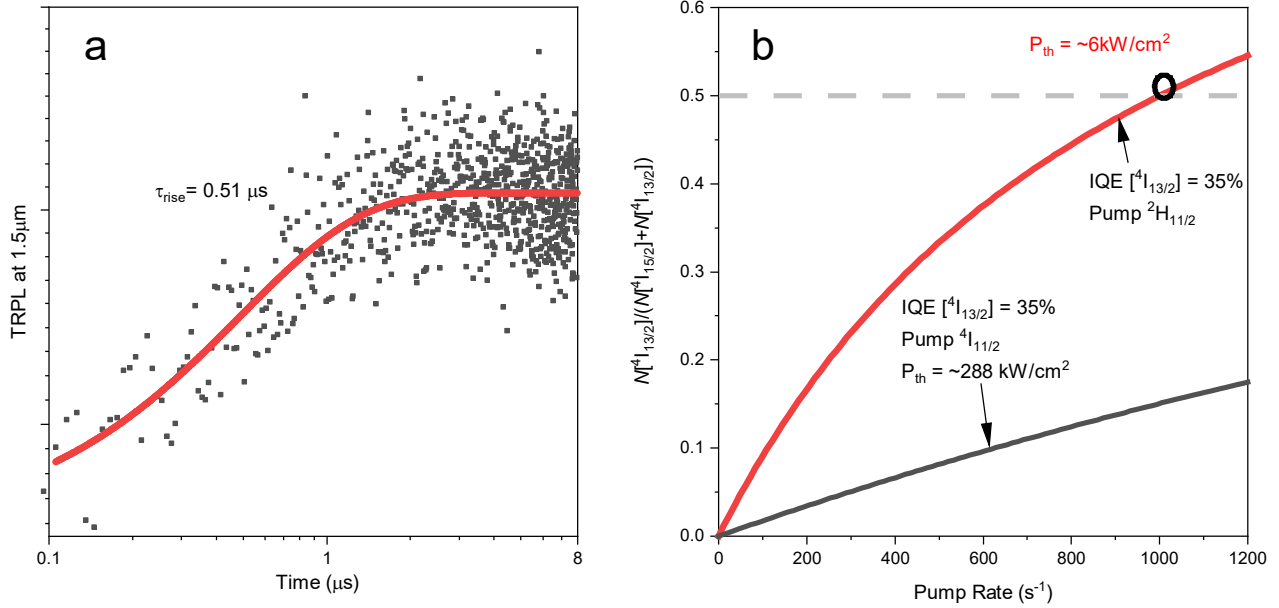


**Figure 4.** (a) TRPL rise time of an encapsulated  $\text{Er}(\text{F-TPIP})_3$  thin film with photoexcitation into  $^2\text{H}_{11/2}$  with a 5ns pulsed 522 nm laser. (b) Comparison of the modelling  $N[{}^4\text{I}_{13/2}]/N[{}^4\text{I}_{15/2}]$  with the nonradiative internal relaxation rates ( $k_{nr}$ ) at the photoexcitation into  ${}^4\text{I}_{11/2}$  and  ${}^2\text{H}_{11/2}$ .

The nonradiative internal relaxations due to overtone couplings results in two advantages for optimizing the optical performance at 1.5  $\mu\text{m}$ . The first is that it allows us to concentrate excited  $\text{Er}^{3+}$  ions onto the  ${}^4\text{I}_{13/2}$  state faster than allowed from the intrinsic transitions. This can be seen in **Figure 4a** where the measured rise time for the  ${}^4\text{I}_{13/2}$  state is  $\sim 0.5 \mu\text{s}$ , compared to a calculated rise time of  $\sim 6 \text{ms}$  (see the SI) for excitation into the  ${}^2\text{H}_{11/2}$  state. This rapid condensing of the excitation onto the  ${}^4\text{I}_{13/2}$  level has a dramatic impact on the pump power required to obtain population inversion. In **Figure 4b**, we plot the ratio of the calculated population of the  ${}^4\text{I}_{13/2}$  and  ${}^4\text{I}_{15/2}$  states, under excitation into the  ${}^2\text{H}_{11/2}$  level, where a value of 0.5 means that population inversion has been achieved. Assuming an IQE of 35% (as we have shown here) we can achieve population inversion at a threshold of  $\sim 6\text{kW}/\text{cm}^2$  compared to  $\sim 100\text{kW}/\text{cm}^2$  which is common for inorganic erbium doped gain media (when pumped into the  ${}^4\text{I}_{11/2}$  level). These values are based on the absorption cross-section for the  ${}^4\text{I}_{15/2} \rightarrow {}^2\text{H}_{11/2}$  transition. However, using an organic chromophore as a sensitizer allows for an  $\sim 10,000$  times

increase in the effective cross-section and implies that this power density can be decreased to  $<1\text{W}/\text{cm}^2$ .<sup>46</sup> The second advantage is that it is possible to eliminate losses due to ETU. For  $\text{Er}^{3+}$  ions, ETU processes are likely excited-state-absorption (ESA) processes with  ${}^4\text{I}_{11/2}$ - ${}^4\text{I}_{11/2}$  or  ${}^4\text{I}_{11/2}$ - ${}^4\text{I}_{13/2}$  interactions and cooperative up-conversion (CUC) with  ${}^4\text{I}_{13/2}$ - ${}^4\text{I}_{13/2}$  interactions. In  $\text{Er}(\text{F-TPIP})_3$ , the overtone vibrations will quench the  ${}^4\text{I}_{11/2}$  state and hence reduce ESA processes and will relax CUC-induced  ${}^4\text{I}_{11/2}$  excitations to the  ${}^4\text{I}_{13/2}$  state instead of the ground  ${}^4\text{I}_{15/2}$  state, meaning that only one excitation is lost instead of two. However, due to the molecular nature of  $\text{Er}(\text{F-TPIP})_3$  it should be stressed that despite the material having an  $\text{Er}^{3+}$  ion concentration of  $\sim 5 \times 10^{20} \text{ cm}^{-3}$  the minimum distance between any two ions is 1.4 nm (limited by the size of the ligand shell) and hence the probability for interactions is reduced compared to inorganic hosts where clustering can occur even at lower ion concentrations.

## Method

The organic complex  $\text{Er}(\text{F-TPIP})_3$  is synthesised according to the published methods. The chemical products of HFTPIP were supplied by Chromosol Ltd.  $\text{ErCl}_3 \cdot 6\text{H}_2\text{O}$  was purchased from Alfa Aesar. The crude material is purified by using a train vacuum purification system. Organic thin films were fabricated in a Chi-Vac UHV thermal evaporation system. The photoluminescence signals are collected by a Horiba Triax 550 spectrometer and detected using a Hamamatsu R5509-72 nitrogen-cooled photomultiplier.

## Supporting Information

Details of absorption measurements, calculation of branching ratios, Förster calculation and rate equation simulation are included in supporting information. Supporting Information is available from the Wiley Online Library or from the author.

## Author Contributions

CL, JG, AW, KZ, RJC, RB, JG and HQY prepared the sample and recorded data. HQY modelled the rate equation simulation. PBW guided the material synthesis. WPG and HQY co-designed the experiment and wrote the paper.

### **Competing interests**

WPG is the founder of Chromosol Ltd which uses these materials to build erbium-based gain regions on to photonic integrated circuits. JG and HQY are employees of Chromosol. PBW is a shareholder in Chromosol.

### **Acknowledgment**

CL was financially supported by the China Scholarship Council and Queen Mary University of London. WPG acknowledges financial support from IUK (79053) and EPSRC (EP/L020114/1 and EP/P007767/1). XPS measurements in this work were performed at the Henry Royce Institute for Advanced Materials, funded through EPSRC grants EP/R00661X/1 and EP/P025021/1.

### **Reference:**

- (1) Fang, Z.; Chen, Q. Y.; Zhao, C. Z. A Review of Recent Progress in Lasers on Silicon. *Optics and Laser Technology*. March 2013, pp 103–110.
- (2) Kelsall, R. W. Rubber Stamp for Silicon Photonics. *Nat. Photonics* **2012**, *6* (September), 577–579.
- (3) Soref, R. The Past, Present, and Future of Silicon Photonics. *IEEE J. Sel. Top. Quantum Electron.* **2006**, *12* (6), 1678–1687.

- (4) Stampoulidis, L.; Vyrsoinos, K.; Voigt, K.; Zimmermann, L.; Gomez-Agis, F.; Dorren, H. J. S.; Sheng, Z.; Van Thourhout, D.; Moerl, L.; Kreissl, J.; et al. The European BOOM Project: Silicon Photonics for High-Capacity Optical Packet Routers. *IEEE J. Sel. Top. Quantum Electron.* **2010**, *16* (5), 1422–1433.
- (5) Frolov, S.; Shen, T.-M.; Bruce, A. J. EDWA: Key Enabler of Optical Integration on PLC. In *Rare-Earth-Doped Materials and Devices VII*; SPIE, 2003; Vol. 4990, p 47.
- (6) Pollnau, M. Rare-Earth-Ion-Doped Waveguide Lasers on a Silicon Chip. In *Optical Components and Materials XII*; SPIE, 2015; Vol. 9359, p 935910.
- (7) Bradley, J. D. B.; Hosseini, E. S.; Purnawirman; Su, Z.; Adam, T. N.; Leake, G.; Coolbaugh, D.; Watts, M. R. Monolithic Erbium- and Ytterbium-Doped Microring Lasers on Silicon Chips. *Opt. Express* **2014**, *22* (10), 12226.
- (8) Patel, F. D.; DiCarolis, S.; Lum, P.; Venkatesh, S.; Miller, J. N. A Compact High-Performance Optical Waveguide Amplifier. *IEEE Photonics Technol. Lett.* **2004**, *16* (12), 2607–2609.
- (9) Agazzi, L.; Bradley, J. D. B.; Dijkstra, M.; Ay, F.; Roelkens, G.; Baets, R.; Wörhoff, K.; Pollnau, M. Monolithic Integration of Erbium-Doped Amplifiers with Silicon-on-Insulator Waveguides. *Opt. Express* **2010**, *18* (26), 27703.
- (10) Bradley, J. D. B.; Pollnau, M. Erbium-Doped Integrated Waveguide Amplifiers and Lasers. *Laser Photon. Rev.* **2011**, *5* (3), 368–403.
- (11) Kik, P. G.; Polman, A. Erbium-Doped Optical-Waveguide Amplifiers on Silicon. *MRS Bull.* **1998**, *23* (4), 48–54.
- (12) Sun, H.; Yin, L.; Liu, Z.; Zheng, Y.; Fan, F.; Zhao, S.; Feng, X.; Li, Y.; Ning, C. Z.

- Giant Optical Gain in a Single-Crystal Erbium Chloride Silicate Nanowire. *Nat. Photonics* **2017**, *11* (9), 589–593.
- (13) Agazzi, L.; Wörhoff, K.; Pollnau, M. Energy-Transfer-Upconversion Models, Their Applicability and Breakdown in the Presence of Spectroscopically Distinct Ion Classes: A Case Study in Amorphous Al<sub>2</sub>O<sub>3</sub>:Er<sup>3+</sup>. *J. Phys. Chem. C* **2013**, *117* (13), 6759–6776.
- (14) Pollnau, M.; Jackson, S. D. Energy Recycling versus Lifetime Quenching in Erbium-Doped 3-Mm Fiber Lasers. *IEEE J. Quantum Electron.* **2002**, *38* (2), 162–169.
- (15) Vázquez-Córdova, S. A.; Dijkstra, M.; Bernhardt, E. H.; Ay, F.; Wörhoff, K.; Herek, J. L.; García-Blanco, S. M.; Pollnau, M. Erbium-Doped Spiral Amplifiers with 20 DB of Net Gain on Silicon. *Opt. Express* **2014**, *22* (21), 25993.
- (16) Kik, P. G.; Polman, A. Cooperative Upconversion as the Gain-Limiting Factor in Er Doped Miniature Al<sub>2</sub>O<sub>3</sub> Optical Waveguide Amplifiers. *J. Appl. Phys.* **2003**, *93* (9), 5008–5012.
- (17) Frankis, H. C.; Mbonde, H. M.; Bonneville, D. B.; Zhang, C.; Mateman, R.; Leinse, A.; Bradley, J. D. B. Erbium-Doped TeO<sub>2</sub>-Coated Si<sub>3</sub>N<sub>4</sub> Waveguide Amplifiers with 5 DB Net Gain. *Photonics Res.* **2020**, *8* (2), 127.
- (18) Belt, M.; Blumenthal, D. J. Erbium-Doped Waveguide DBR and DFB Laser Arrays Integrated within an Ultra-Low-Loss Si<sub>3</sub>N<sub>4</sub> Platform. *Opt. Express* **2014**, *22* (9), 10655.
- (19) Purnawirman; Sun, J.; Adam, T. N.; Leake, G.; Coolbaugh, D.; Bradley, J. D. B.; Hosseini, E. S.; Watts, M. R. C- and L-Band Erbium-Doped Waveguide Lasers with Wafer-Scale Silicon Nitride Cavities. *Opt. Lett.* **2013**, *38* (11), 1760.

- (20) Hernández, I.; Gillin, W. P. Organic Chromophores-Based Sensitization of NIR-Emitting Lanthanides: Toward Highly Efficient Halogenated Environments. In *Handbook on the Physics and Chemistry of Rare Earths*; Elsevier, 2015; Vol. 47, pp 1–100.
- (21) Bünzli, J.-C. G. On the Design of Highly Luminescent Lanthanide Complexes. *Coord. Chem. Rev.* **2015**, 293–294, 19–47.
- (22) Zou, W.; Visser, C.; Maduro, J. A.; Pshenichnikov, M. S.; Hummelen, J. C. Broadband Dye-Sensitized Upconversion of near-Infrared Light. *Nat. Photonics* **2012**, 6 (8), 560–564.
- (23) Wang, T.; Zhao, D.; Zhang, M.; Yin, J.; Song, W.; Jia, Z.; Wang, X.; Qin, G.; Qin, W.; Wang, F.; et al. Optical Waveguide Amplifiers Based on NaYF<sub>4</sub>: Er<sup>3+</sup>, Yb<sup>3+</sup> NPs-PMMA Covalent-Linking Nanocomposites. *Opt. Mater. Express* **2015**, 5 (3), 469.
- (24) Ashoka Sahadevan, S.; Monni, N.; Abhervé, A.; Marongiu, D.; Sarritzu, V.; Sestu, N.; Saba, M.; Mura, A.; Bongiovanni, G.; Cannas, C.; et al. Nanosheets of Two-Dimensional Neutral Coordination Polymers Based on Near-Infrared-Emitting Lanthanides and a Chlorocyananilate Ligand. *Chem. Mater.* **2018**, 30 (18), 6575–6586.
- (25) Chen, P.-Z.; Zhang, H.; Niu, L.-Y.; Zhang, Y.; Chen, Y.-Z.; Fu, H.-B.; Yang, Q.-Z. A Solid-State Fluorescent Material Based on Carbazole-Containing Difluoroboron  $\beta$ -Diketonate: Multiple Chromisms, the Self-Assembly Behavior, and Optical Waveguides. *Adv. Funct. Mater.* **2017**, 27 (25), 1700332.
- (26) Davis, D.; Carrod, A. J.; Guo, Z.; Kariuki, B. M.; Zhang, Y. Z.; Pikramenou, Z. Imidodiphosphate Ligands for Enhanced Sensitization and Shielding of Visible and Near-Infrared Lanthanides. *Inorg. Chem.* **2019**, 58 (19), 13268–13275.



- (27) Martín-Ramos, P.; Martín, I. R.; Lahoz, F.; Hernández-Navarro, S.; Pereira Da Silva, P. S.; Hernández-Campo, I.; Lavín, V.; Ramos Silva, M. An Erbium(III)-Based NIR Emitter with a Highly Conjugated  $\beta$ -Diketonate for Blue-Region Sensitization. *J. Alloys Compd.* **2015**, *619*, 553–559.
- (28) Ye, H. Q.; Li, Z.; Peng, Y.; Wang, C. C.; Li, T. Y.; Zheng, Y. X.; Sapelkin, A.; Adamopoulos, G.; Hernández, I.; Wyatt, P. B.; et al. Organo-Erbium Systems for Optical Amplification at Telecommunications Wavelengths. *Nat. Mater.* **2014**, *13* (4), 382–386.
- (29) Binnemans, K. Lanthanide-Based Luminescent Hybrid Materials | Koen Binnemans - Academia.Edu. *Chem. Rev.* **2009**, *109*, 4283–4374.
- (30) Li, H. F.; Liu, X. Q.; Lyu, C.; Gorbaciova, J.; Wen, L. L.; Shan, G. G.; Wyatt, P. B.; Ye, H. Q.; Gillin, W. P. Enhanced 1.54-Mm Photo- and Electroluminescence Based on a Perfluorinated Er(III) Complex Utilizing an Iridium(III) Complex as a Sensitizer. *Light Sci. Appl.* **2020**, *9* (1), 1–10.
- (31) Zhang, D.; Li, W.; Chu, B.; Li, X.; Han, L.; Zhu, J.; Li, T.; Bi, D.; Yang, D.; Yan, F.; et al. Sensitized Photo- and Electroluminescence from Er Complexes Mixed with Ir Complex. *Appl. Phys. Lett.* **2008**, *92* (9), 093501.
- (32) Winkless, L.; Tan, R. H. C. C.; Zheng, Y.; Motevalli, M.; Wyatt, P. B.; Gillin, W. P. Quenching of Er (III) Luminescence by Ligand CH Vibrations: Implications for the Use of Erbium Complexes in Telecommunications. *Appl. Phys. Lett.* **2006**, *89* (11), 1115.
- (33) Doffek, C.; Alzakhem, N.; Bischof, C.; Wahsner, J.; Güden-Silber, T.; Lügger, J.; Platas-Iglesias, C.; Seitz, M. Understanding the Quenching Effects of Aromatic C-H- and C-D-Oscillators in near-IR Lanthanoid Luminescence. *J. Am. Chem. Soc.* **2012**, *134*

- (39), 16413–16423.
- (34) Glover, P. B.; Bassett, A. P.; Nockemann, P.; Kariuki, B. M.; Van Deun, R.; Pikramenou, Z. Fully Fluorinated Imidodiphosphate Shells for Visible- and NIR-Emitting Lanthanides: Hitherto Unexpected Effects of Sensitizer Fluorination on Lanthanide Emission Properties. *Chem. - A Eur. J.* **2007**, *13* (22), 6308–6320.
- (35) Shavaleev, N. M.; Scopelliti, R.; Gumy, F.; Bünzli, J. C. G. Surprisingly Bright Near-Infrared Luminescence and Short Radiative Lifetimes of Ytterbium in Hetero-Binuclear Yb-Na Chelates. *Inorg. Chem.* **2009**, *48* (16), 7937–7946.
- (36) Ye, H. Q.; Peng, Y.; Li, Z.; Wang, C. C.; Zheng, Y. X.; Motevalli, M.; Wyatt, P. B.; Gillin, W. P.; Hernández, I. Effect of Fluorination on the Radiative Properties of Er<sup>3+</sup> Organic Complexes: An Opto-Structural Correlation Study. *J. Phys. Chem. C* **2013**, *117* (45), 23970–23975.
- (37) Ye, H.; Bogdanov, V.; Liu, S.; Vajandar, S.; Osipowicz, T.; Hernández, I.; Xiong, Q. Bright Photon Upconversion on Composite Organic Lanthanide Molecules through Localized Thermal Radiation. *J. Phys. Chem. Lett.* **2017**, *8* (23), 5695–5699.
- (38) Sardar, D. K.; Gruber, J. B.; Zandi, B.; Hutchinson, J. A.; Ward Trussell, C. Judd-Ofelt Analysis of the Er<sup>3+</sup>(<sup>4</sup>f<sub>11</sub>) Absorption Intensities in Phosphate Glass: Er<sup>3+</sup>, Yb<sup>3+</sup>. *J. Appl. Phys.* **2003**, *93* (4), 2041–2046.
- (39) Li, A.; Sun, L.; Zheng, Z.; Wu, W.; Liu, W.; Yang, Y.; Lü, T.; Su, W. Spectroscopic Analysis of Er<sup>3+</sup> Transition in Mg/Er-Codoped LiNbO<sub>3</sub> Crystal. *J. Lumin.* **2008**, *128* (2), 239–244.
- (40) Desirena, H.; De La Rosa, E.; Díaz-Torres, L. A.; Kumar, G. A. Concentration Effect of

- Er<sup>3+</sup> Ion on the Spectroscopic Properties of Er<sup>3+</sup> and Yb<sup>3+</sup>/Er<sup>3+</sup> Co-Doped Phosphate Glasses. *Opt. Mater. (Amst)*. **2006**, 28 (5), 560–568.
- (41) Reddy, K. V.; Heller, D. F.; Berry, M. J. Highly Vibrationally Excited Benzene: Overtone Spectroscopy and Intramolecular Dynamics of C<sub>6</sub>H<sub>6</sub>, C<sub>6</sub>D<sub>6</sub>, and Partially Deuterated or Substituted Benzenes. *J. Chem. Phys.* **1982**, 76 (6), 2814–2837.
- (42) Koszykowski, M. L.; Nold, D. W.; Marcus, R. A. *Semiclassical Theory of Intensities of Vibrational Fundamentals, Overtones, and Combination Bands*; 1982; Vol. 86.
- (43) Etzkorn, T.; Klotz, B.; Sørensen, S.; Patroescu, I. V.; Barnes, I.; Becker, K. H.; Platt, U. Gas-Phase Absorption Cross Sections of 24 Monocyclic Aromatic Hydrocarbons in the UV and IR Spectral Ranges. *Atmos. Environ.* **1999**, 33 (4), 525–540.
- (44) Phillips, J. A.; Orlando, J. J.; Tyndall, G. S.; Vaida, V. Integrated Intensities of OH Vibrational Overtones in Alcohols. *Chem. Phys. Lett.* **1998**, 296 (3–4), 377–383.
- (45) Mulak, J.; Mulak, M. Capability of the Free-Ion Eigenstates for Crystal-Field Splitting. *J. Mod. Phys.* **2011**, 02 (11), 1373–1389.
- (46) Hu, J. X.; Karamshuk, S.; Gorbaciova, J.; Ye, H. Q.; Lu, H.; Zhang, Y. P.; Zheng, Y. X.; Liang, X.; Hernández, I.; Wyatt, P. B.; et al. High Sensitization Efficiency and Energy Transfer Routes for Population Inversion at Low Pump Intensity in Er Organic Complexes for IR Amplification. *Sci. Rep.* **2018**, 8 (1), 3226.